PHYSICAL REVIEW B **99**, 035151 (2019)

Adiabatic generalized gradient approximation kernel in time-dependent density functional theory

N. Singh,[1,2,3,*] P. Elliott,[1] T. Nautiyal,[2] J. K. Dewhurst,[1] and S. Sharma[3,2]
[1]*Max-Planck-Institut für Mikrostrukturphysik, Weinberg 2, D-06120 Halle, Germany*
[2]*Department of Physics, Indian Institute of Technology-Roorkee, 247667 Uttarakhand, India*
[3]*Max-Born-Institut für Nichtlineare Optik und Kurzzeitspektroskopie, Max-Born-Strasse 2A, 12489 Berlin, Germany*

(Received 1 August 2018; revised manuscript received 21 November 2018; published 25 January 2019)

A complete understanding of a material requires both knowledge of the excited states as well as of the ground state. In particular, the low energy excitations are of utmost importance while studying the electronic, magnetic, dynamical, and thermodynamical properties of the material. Time-dependent density functional theory (TDDFT), within the linear regime, is a successful *ab initio* method to assess the electronic charge and spin excitations. However, it requires an approximation to the exchange-correlation (XC) kernel which encapsulates the effect of electron-electron interactions in the many-body system. In this work we derive and implement the spin-polarized XC kernel for semilocal approximation, the so-called adiabatic generalized gradient approximation (AGGA). This kernel has a quadratic dependence on the wave vector $\mathbf{q}$ of the perturbation, however the impact of this on the electron energy loss spectra (EELS) is small. We show that the AGGA generally worsens the spin-excitation spectra by overestimating the magnon energies and suppressing the intensity of spin waves.

DOI: 10.1103/PhysRevB.99.035151

I. INTRODUCTION

Recent developments in the field of laser-induced spin dynamics have opened up the world of *femtomagnetism* [1], whereby the spin degree-of-freedom is controlled using ultrafast laser pulses [2]. As the name suggests, femtomagnetism concerns charge and spin dynamics on the femtosecond ($=10^{-15}$ s) time scale, corresponding to energies in the meV range. Electronic excitations in this energy regime can be classified as either *single-particle* like, e.g., Stoner spin flips, or *collective* in nature, e.g., charge density waves [3], excitons, or magnons [4]. Long wavelength collective excitations occur at relatively lower energies as compared to the single-particle excitations. To exploit the vast potential femtomagnetism offers, it is vital that we are able to accurately describe these excitations in order to understand, and ultimately control, them.

Theoretical studies of spin excitations can be performed using either simple models like the Landau-Lifshitz-Gilbert equation [5], Heisenberg model [6], etc., or computationally more demanding, parameter-free, *ab initio* methods. In contrast to *ab initio* methods, model based approaches are limited by their lack of generality, as they are usually tailored to study only specific problems and cannot be applied universally.

Time dependent density functional theory (TDDFT) [7–9] is an *ab initio* method which can predict the excited state properties of materials. Since its theoretical foundation in 1984 [7], it has been successfully applied to study excited state properties of a wide range of materials [10,11]. Compared to other *ab initio* methods, such as many-body perturbation theory (MBPT), TDDFT provides a similar level of accuracy but at far less computational cost.

The evolution of electronic charge and spin densities is calculated using TDDFT by solving the single-particle Kohn-Sham (KS) equations. The effects of electron-electron interactions come into this noninteracting KS system via an effective potential, the so-called Hartree exchange-correlation (XC) potential. Although TDDFT is an exact theory for treating systems under the influence of strong time-dependent external potentials [12–19], it is most commonly applied within the weak perturbation limit. When working in this linear regime, one requires the functional derivative of the XC potential, the so-called XC kernel. In a practical TDDFT calculation, an approximation to the XC potential and the kernel is required.

There are many different flavors of XC energy functionals in ground-state DFT, which can be divided into the local density approximation (LDA), generalized gradient approximations (GGAs), meta-GGAs, hybrids, and Fock-like approximations, comprising the so-called *Jacob's ladder* [20] of approximations, where the level of accuracy increases as we climb from LDA to hybrids. The performance of these approximations in static ground-state DFT has been well studied, however much less is known about their behavior in TDDFT. This is an active research field, involving development of functionals, including those with adiabatic approximation, and going beyond the adiabatic approximation [21–24]. Most of the research deals with the optical absorption spectra, and, in particular, the failure of simple XC kernels to predict bound excitons. From these studies, we know the importance of describing the long wavelength limit of the XC kernel correctly in order to obtain reasonable exciton binding energies, leading to a number of new approximations [25–33]. However for magnetic excitations, only the ALDA XC kernel within the framework of TDDFT has been properly studied, e.g., for calculations of the magnon spectra [34–36], where for many cases it overestimates magnon energies as compared to experiments. Besides TDDFT, many-body perturbation theory can be used [37,38] to calculate magnon spectra. Additionally, time-dependent generalization of all-electron Sternheimer

---

[*] nisha.singh@mpi-halle.mpg.de

approach [39] or exchange parameters [36,40] extracted from ground state DFT calculations can also be used to calculate the magnon spectra.

For the static DFT, it is well known that going from LDA to GGA improves many ground state properties [41]. Hence, in the work presented here, we climb up to the next rung of *Jacobs's Ladder* within TDDFT and ask if including gradient corrections to the XC kernel improves the charge and spin excitation spectra. The paper is organized as follows: Section II gives the basic equations of TDDFT and how they may be used to calculate excitation energies via the linear-response susceptibilities. We will also derive the adiabatic GGA (AGGA) XC kernel for noncollinear spin systems in this section. In Sec. III, we apply the AGGA kernel to first study the electron energy loss spectra (EELS) for medium- (diamond) and large- (LiF) band-gap insulators. A comparison is made with experiments and the ALDA kernel. Then a more comprehensive study is made for magnetic excitations of simple bulk ferromagnetic systems Fe, Co, and Ni, and Heusler and half-Heusler materials. Again we compare with experimental data, as well as previous theoretical works. Finally, in Sec. IV, we give some concluding remarks on the performance of AGGA.

II. THEORETICAL FORMULATION

When the external perturbation is small, the response of the system to this stimulus can be studied through a suitable linear response function and can be expanded in a Taylor series with respect to the perturbation. The coefficients of this expansion are the response functions which have useful information embedded in them, such as the optical absorption spectra, Pockels effect, optical rectification, second harmonic generation, Kerr effect, etc. In this paper we primarily focus on the first order response functions (the so-called linear response) and particularly on the charge-charge response ($\delta\rho/\delta v_{\text{ext}}$) and the spin-spin response ($\delta\mathbf{m}/\delta\mathbf{B}_{\text{ext}}$), where $\rho(\mathbf{r},t)$, $v_{\text{ext}}(\mathbf{r},t)$, $\mathbf{m}(\mathbf{r},t)$, $\mathbf{B}_{\text{ext}}(\mathbf{r},t)$ correspond to the charge density, electric scalar potential, magnetization density, and magnetic field, respectively. For noncollinear systems, the fully interacting response function is defined as:

$$\chi^{\mu\nu}(\mathbf{r},\mathbf{r}',t-t') = \frac{\delta\rho^{\mu}(\mathbf{r},t)}{\delta V^{\nu}_{\text{ext}}(\mathbf{r}',t')}, \qquad (1)$$

where $\rho^{\mu=0;1-3} = [\rho,\mathbf{m}]$, $V^{\nu=0;1-3}_{\text{ext}} = [v_{\text{ext}},\mathbf{B}_{\text{ext}}]$. χ is a 4×4 matrix [42,43] of matrices as shown in Fig. 1. When calculating linear response of a stationary state, we can fourier transform χ to frequency space.

The noninteracting KS linear response functions can be derived, in terms of the KS spinors $\phi(\mathbf{r})$, using first-order perturbation theory:

$$\chi_0^{\mu\nu}(\mathbf{r},\mathbf{r}',\omega) = \lim_{\eta\to0}\sum_{\kappa}\sum_{\xi}\sigma^{\mu}\sigma^{\nu}(f_\kappa - f_\xi) \times \frac{\phi^*_\kappa(\mathbf{r})\phi_\xi(\mathbf{r})\phi_\kappa(\mathbf{r}')\phi^*_\xi(\mathbf{r}')}{\omega+(\varepsilon_\kappa-\varepsilon_\xi)+i\eta}, \qquad (2)$$

where κ,ξ are joint indices for the state and band, f_κ, f_ξ denote the Kohn-Sham occupation numbers, respectively, and $\sigma^{\mu} = [\mathbb{I},\sigma^{x,y,z}]$ are the Pauli spin matrices with $\mathbb{I}$ being the identity matrix. For convenience, Einstein summation is used from here on.

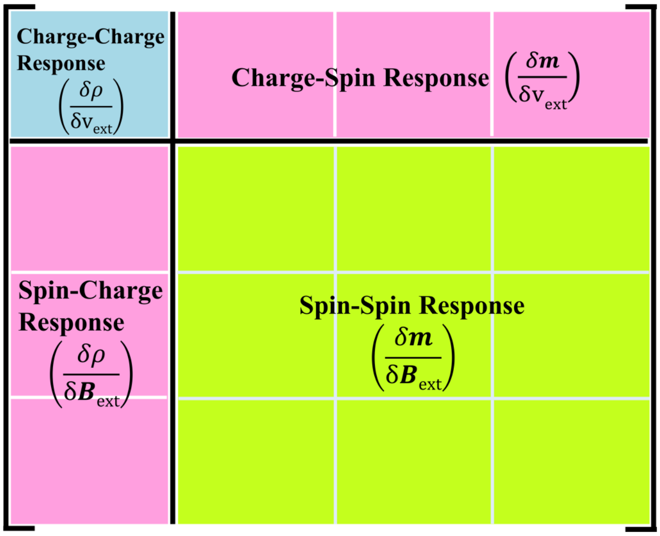

FIG. 1. The structure of the fully interacting and noninteracting response functions.

TDDFT relates this noninteracting response function of the KS system to that of the interacting system via a Dyson-like equation (in fourier space):

$$\chi^{\mu\nu}(\mathbf{r},\mathbf{r}',\omega) = \chi_0^{\mu\nu}(\mathbf{r},\mathbf{r}',\omega) + \int d^3r'' \int d^3r'''\chi_0^{\mu\delta}(\mathbf{r},\mathbf{r}'',\omega)\big[f_{\text{H}}^{\delta\gamma}(\mathbf{r}'',\mathbf{r}''') + f_{\text{XC}}^{\delta\gamma}(\mathbf{r}'',\mathbf{r}''',\omega)\big]\chi^{\gamma\nu}(\mathbf{r}''',\mathbf{r}',\omega), \qquad (3)$$

where $f_{\text{H}}^{\mu\nu}(\mathbf{r},\mathbf{r}') = \delta^{\mu0}\delta^{\nu0}v(\mathbf{r},\mathbf{r}')$ is the Hartree kernel, $v(\mathbf{r},\mathbf{r}') = 1/|\mathbf{r}-\mathbf{r}'|$ is the Coulomb potential, ω corresponds to frequency, and $f_{\text{XC}}^{\mu\nu}(\mathbf{r},\mathbf{r}',\omega)$ is the XC kernel, which is the Fourier transform of:

$$f_{\text{XC}}^{\mu\nu}(\mathbf{r},t,\mathbf{r}',t') = \frac{\delta V^{\mu}_{\text{XC}}(\mathbf{r},t)}{\delta\rho^{\nu}(\mathbf{r}',t')}, \qquad (4)$$

where $V_{\text{XC}}^{\mu=0;1-3} = [v_{\text{XC}},\mathbf{B}_{\text{XC}}]$ is the combined XC potential for the scalar field v_{XC} and vector field $\mathbf{B}_{\text{XC}}$.

Since it is convenient to work in reciprocal space for periodic systems, all quantities are represented as matrices in reciprocal space vectors $\mathbf{G}$. The Fourier transformed interacting response has the form:

$$\chi^{\mu\nu}_{\mathbf{G},\mathbf{G}'}(\mathbf{q},\omega) = \int\int e^{-i(\mathbf{q}+\mathbf{G})\cdot\mathbf{r}}\chi^{\mu\nu}(\mathbf{r},\mathbf{r}',\omega)e^{i(\mathbf{q}+\mathbf{G}')\cdot\mathbf{r}'}d^3r\,d^3r'. \qquad (5)$$

Here $\mathbf{G}$, $\mathbf{G}'$ are the reciprocal lattice vectors and $\mathbf{q}$ is the wave vector of the perturbation.

Conventionally, the excitations are studied in the decoupled limit where the off-diagonal terms of Fig. 1 are set to zero (i.e., $\delta\mathbf{m}/\delta v_{\text{ext}} = 0 = \delta\rho/\delta\mathbf{B}_{\text{ext}}$). This allows us to separate the dielectric response and magnetic response.

Experimental observables may then be extracted from the response functions, for example, the inverse dielectric function is

$$\epsilon^{-1}_{\mathbf{G},\mathbf{G}'}(\mathbf{q},\omega)=\delta_{\mathbf{G},\mathbf{G}'}+\left(\frac{4\pi}{\mathbf{q}^2}\right)\chi^{00}_{\mathbf{G},\mathbf{G}'}(\mathbf{q},\omega). \tag{6}$$

The imaginary part of ϵ^{-1} gives the EELS whereas the imaginary part of ϵ gives the absorption spectrum. Likewise, the neutron scattering cross section is proportional to the transverse magnetic response [44]

$$\frac{d^2\sigma}{d\Omega d\omega}\propto\bigg\{\left(1-\kappa_z^2\right)Im[\chi^{zz}(\mathbf{q},\omega)] + \frac{1}{4}\left(1-\kappa_z^2\right)Im[\chi^{-+}(\mathbf{q},\omega)+\chi^{+-}(\mathbf{q},\omega)]\bigg\}, \tag{7}$$

where $\kappa_z=(\mathbf{k}_f-\mathbf{k}_i)_z/|\mathbf{k}_f-\mathbf{k}_i|$ is related to the $\mathbf{q}$ vector through $\mathbf{q}=\mathbf{k}_f-\mathbf{k}_i$ and is folded back into the first Brillouin zone (BZ). Here, the transverse terms comprise $\chi^{-+}(=2\chi^{xx}+2i\chi^{xy})$ and $\chi^{+-}(=2\chi^{xx}-2i\chi^{xy})$. The term χ^{zz} does not contribute to the spin-flip excitations, rather it is the transverse terms of the magnetic susceptibility which give rise to the Stoner and magnon excitations.

A. GGA kernel

Within DFT, interactions between the electrons are encapsulated in the XC potential. However, the exact form of v_{xc} is not known and approximations are required for all practical calculations. For linear response studies using time dependent extension of DFT, one requires the functional derivative of this v_{xc} w.r.t. the density (i.e., the XC kernel). Here we will derive the XC kernel for GGA functionals within the adiabatic approximation (AA). This kernel is semilocal in space and local in time; for the spin unpolarized case, the XC energy functional, E_{xc}, depends not only on the density, $n(\mathbf{r})$, but also on its gradient, $\nabla n(\mathbf{r})$, at each point $\mathbf{r}$ in space. The XC potential and kernel can be obtained from first and second order functional derivatives, respectively, of E_{xc} with respect to the density, i.e.,

$$v_{\mathrm{xc}}[\rho](\mathbf{r})=\frac{\delta E_{\mathrm{xc}}[\rho]}{\delta\rho(\mathbf{r})} \tag{8}$$

$$f_{\mathrm{xc}}[\rho](\mathbf{r},\mathbf{r}')=\frac{\delta^2 E_{\mathrm{xc}}[\rho]}{\delta\rho(\mathbf{r})\delta\rho(\mathbf{r}')}, \tag{9}$$

where $E_{\mathrm{xc}}[\rho]=\int e_{\mathrm{xc}}(\rho,\nabla\rho)(\vec{r})d^3r$ for the GGA functional and e_{xc} is the XC energy density.

The variation of the XC energy is defined by:

$$\begin{aligned}\delta E_{\mathrm{xc}}&=E_{\mathrm{xc}}[\rho+\delta\rho]-E_{\mathrm{xc}}[\rho]\\&=\int v_{\mathrm{xc}}[\rho](\mathbf{r})\delta\rho(\mathbf{r})d^3r\\&\quad+\frac{1}{2}\int\int f_{\mathrm{xc}}[\rho](\mathbf{r},\mathbf{r}')\delta\rho(\mathbf{r})\delta\rho(\mathbf{r}')d^3rd^3r'+\cdots\end{aligned} \tag{10}$$

Taylor expanding the energy density up to first order gives

$$\begin{aligned}&e_{\mathrm{xc}}(\rho+\delta\rho,\nabla\rho+\nabla\delta\rho)(\mathbf{r})\\&=e_{\mathrm{xc}}(\rho,\nabla\rho)(\mathbf{r})+\frac{\partial e_{\mathrm{xc}}(\rho,\nabla\rho)}{\partial\rho}(\mathbf{r})\delta\rho(\mathbf{r})\\&\quad+\frac{\partial e_{\mathrm{xc}}(\rho,\nabla\rho)}{\partial\nabla\rho}(\mathbf{r})\cdot\nabla\delta\rho(\mathbf{r})\end{aligned} \tag{11}$$

leading to the expansion of energy functional,

$$\begin{aligned}&E_{\mathrm{xc}}[\rho+\delta\rho,\nabla\rho+\nabla\delta\rho]\\&=E_{\mathrm{xc}}[\rho,\nabla\rho]+\int d^3r\frac{\partial e_{\mathrm{xc}}(\rho,\nabla\rho)}{\partial\rho}(\mathbf{r})\delta\rho(\mathbf{r})\\&\quad+\int d^3r\frac{\partial e_{\mathrm{xc}}(\rho,\nabla\rho)}{\partial\nabla\rho}(\mathbf{r})\cdot\nabla\delta\rho(\mathbf{r})\end{aligned} \tag{12}$$

and

$$\begin{aligned}\delta E_{\mathrm{xc}}=\int d^3r\bigg[&\frac{\partial e_{\mathrm{xc}}(\rho,\nabla\rho)}{\partial\rho}(\mathbf{r})\delta\rho(\mathbf{r})\\&+\frac{\partial e_{\mathrm{xc}}(\rho,\nabla\rho)}{\partial\nabla\rho}(\mathbf{r})\cdot\nabla\delta\rho(\mathbf{r})\bigg].\end{aligned} \tag{13}$$

Carrying out integration by parts of the second term gives us:

$$\begin{aligned}\delta E_{\mathrm{xc}}=\int d^3r\bigg[&\frac{\partial e_{\mathrm{xc}}(\rho,\nabla\rho)}{\partial\rho}(\mathbf{r})\\&-\left\{\nabla\cdot\frac{\partial e_{\mathrm{xc}}(\rho,\nabla\rho)}{\partial\nabla\rho}(\mathbf{r})\right\}\bigg]\delta\rho(\mathbf{r}).\end{aligned} \tag{14}$$

Comparing Eq. (14) with Eq. (10), we find the XC potential as:

$$\begin{aligned}v_{\mathrm{xc}}[\rho](\mathbf{r})&=\frac{\partial e_{\mathrm{xc}}(\rho,\nabla\rho)}{\partial\rho}(\mathbf{r})-\left\{\nabla\cdot\frac{\partial e_{\mathrm{xc}}(\rho,\nabla\rho)}{\partial\nabla\rho}(\mathbf{r})\right\}\\&=\frac{\partial e_{\mathrm{xc}}(\rho,\nabla\rho)}{\partial\rho}(\mathbf{r})\\&\quad-2\left\{\nabla\cdot\left(\frac{\partial e_{\mathrm{xc}}(\rho,\nabla\rho)}{\partial\sigma}(\mathbf{r})\nabla\rho\right)\right\},\end{aligned} \tag{15}$$

where $\sigma=\nabla\rho\cdot\nabla\rho$ is often used in practice. Variation of this potential to first order will give the kernel:

$$\begin{aligned}\delta v_{\mathrm{xc}}(\mathbf{r})&=v_{\mathrm{xc}}[\rho+\delta\rho,\nabla\rho+\nabla\delta\rho](\mathbf{r})-v_{\mathrm{xc}}[\rho,\nabla\rho](\mathbf{r})\\&=\frac{\partial^2 e_{\mathrm{xc}}}{\partial\rho^2}(\mathbf{r})\delta\rho(\mathbf{r})+\frac{\partial^2 e_{\mathrm{xc}}}{\partial\nabla_j\rho\partial\rho}(\mathbf{r})\nabla_j\delta\rho(\mathbf{r})\\&\quad-\nabla_k\bigg[\frac{\partial^2 e_{\mathrm{xc}}}{\partial\rho\partial\nabla_k\rho}(\mathbf{r})\delta\rho(\mathbf{r})\\&\quad+\frac{\partial^2 e_{\mathrm{xc}}}{\partial\nabla_j\rho\partial\nabla_k\rho}(\mathbf{r})\nabla_j\delta\rho(\mathbf{r})\bigg].\end{aligned} \tag{16}$$

Integrating these terms individually by introducing a delta function gives us the kernel for GGA functional [33,45,46]

$$\begin{aligned}f_{\mathrm{xc}}(\mathbf{r},\mathbf{r}')&=\delta(\mathbf{r}-\mathbf{r}')\left[\frac{\partial^2 e_{\mathrm{xc}}}{\partial\rho\partial\rho}(\mathbf{r}')-\nabla'_j\frac{\partial^2 e_{\mathrm{xc}}}{\partial\nabla_j\rho\partial\rho}(\mathbf{r}')\right]\\&\quad-\nabla'_j\left[[\nabla'_k\delta(\mathbf{r}-\mathbf{r}')]\frac{\partial^2 e_{\mathrm{xc}}}{\partial\nabla_j\rho\partial\nabla_k\rho}(\mathbf{r}')\right].\end{aligned} \tag{17}$$

Repeating the above derivation for the spin polarized case (see Appendix) gives us two equations comprising the symmetric terms $f^{\alpha\alpha}_{\mathrm{xc}}(\mathbf{r},\mathbf{r}')$, $f^{\beta\beta}_{\mathrm{xc}}(\mathbf{r},\mathbf{r}')$ and the asymmetric terms $f^{\alpha\beta}_{\mathrm{xc}}(\mathbf{r},\mathbf{r}')=f^{\beta\alpha}_{\mathrm{xc}}(\mathbf{r}',\mathbf{r})$ of the XC kernel matrix, where α and

β label the up and down spins, respectively,

$$f_{\mathrm{XC}}^{\alpha\alpha}(\mathbf{r},\mathbf{r}') = \delta(\mathbf{r}-\mathbf{r}')\left[\frac{\partial^2 e_{\mathrm{XC}}}{\partial\rho_\alpha\partial\rho_\alpha}(\mathbf{r}') - \nabla'_k\frac{\partial^2 e_{\mathrm{XC}}}{\partial\nabla_k\rho_\alpha\partial\rho_\alpha}(\mathbf{r}')\right] - \nabla'_k\left[[\nabla'_j\delta(\mathbf{r}-\mathbf{r}')]\left(\frac{\partial^2 e_{\mathrm{XC}}}{\partial\nabla_k\rho_\alpha\partial\nabla_j\rho_\alpha}(\mathbf{r}')\right)\right] \quad (18)$$

$$\begin{aligned} f_{\mathrm{XC}}^{\alpha\beta}(\mathbf{r},\mathbf{r}') = {} & \delta(\mathbf{r}-\mathbf{r}')\left\{\frac{\partial^2 e_{\mathrm{XC}}}{\partial\rho_\beta\partial\rho_\alpha}(\mathbf{r}')\right\} \\ & - \left\{[\nabla'_j\delta(\mathbf{r}-\mathbf{r}')]\left(\frac{\partial^2 e_{\mathrm{XC}}}{\partial\rho_\alpha\partial\nabla_j\rho_\beta}(\mathbf{r})\right)\right\} \\ & + \left\{[\nabla'_j\delta(\mathbf{r}-\mathbf{r}')]\left(\frac{\partial^2 e_{\mathrm{XC}}}{\partial\rho_\beta\partial\nabla_j\rho_\alpha}(\mathbf{r}')\right)\right\} \\ & - \nabla'_k\left\{[\nabla'_j\delta(\mathbf{r}-\mathbf{r}')]\left(\frac{\partial^2 e_{\mathrm{XC}}}{\partial\nabla_k\rho_\beta\partial\nabla_j\rho_\alpha}(\mathbf{r}')\right)\right\} \end{aligned} \quad (19)$$

which is extended to noncollinear cases by using the Kübler's method [47], see Eqs. (A9)–(A12).

III. COMPUTATIONAL DETAILS

All calculations are performed using the all-electron full-potential linearized augmented plane wave electronic structure code ELK [48] with PW91 (LDA) [49] and PBE (GGA) [50] functionals. For diamond and LiF, a fcc crystal structure with experimental lattice spacings of 3.56 Å and 4.02 Å, respectively, is used. A dense k-point grid is required to obtain the response functions, hence the BZ is sampled on a k-point grid of 25 × 25 × 25 for both. The interstitial density and potential are expanded in a **G**-point grid of size 36 × 36 × 36 and the response is calculated using **G** vectors of length 4 Bohr^{-1}. The number of conduction bands included in calculation are 20 for LiF and 36 for diamond. The method to obtain response functions is a two-step procedure, firstly a ground-state calculation is done to obtain the converged density and potentials. The scissor operator has been used to correct the optical band gap by 1.306 eV and 5.06 eV for diamond and LiF, respectively. Then the EELS spectra of LiF and diamond are obtained from the LDA and GGA kernels using the corrected band gaps.

The magnon spectra are highly sensitive to a number of parameters, hence convergence has to be checked with respect to the **k**-point grid and the number of **G** vectors. In these calculations we have used a 40 × 40 × 40 **k**-point grid. The response functions are expanded in **G** space with the length of **G** vector up to 6 Bohr^{-1}. States up to 30 eV above the Fermi level are included for calculation of the response function. A smearing parameter, η, with the value 0.027 eV has been used to smear out the delta function at the excitation energies. The experimental lattice constant used for Co$_2$MnSi is 5.640 [51] Å and for NiMnSb [52] is 5.897 Å. Additional high convergence parameters for magnon spectra were used: (1) the maximum length of $|\mathbf{G}|$ for expanding the interstitial density and potential as 12 Bohr^{-1} and (2) R^{MT} × max$|\mathbf{G}+\mathbf{k}|$ as 8. These parameters resulted in minimum Goldstone error and then the spectra was shifted to satisfy the Goldstone theorem.

IV. RESULTS

A. Semiconductor spectra

It is well known that the **q**-dependent behavior of the XC kernel is of vital importance for predicting the optical response of materials. For example, in the long-wavelength limit ($\mathbf{q} \to 0$), the XC kernel must go as $1/\mathbf{q}^2$ in order to capture excitonic effects [8,11,29,32,59,60]. However, the first rung on *Jacob's ladder*, the ALDA, does not display any **q** dependence, owing to the local approximation for the XC energy. This explains why ALDA does not yield excitonic peaks [8]. The second rung consists of semilocal functionals which include information not just about the density but also its gradients. In this case, it has been shown that the AGGA kernel shows $\mathbf{q}^2$ behavior [61]. Hence we explore if this has any impact on the EELS spectra.

In Fig. 2(a) we plot the EELS for (i) LiF, which is a large band-gap material with a bound exciton and (ii) diamond which is a medium band-gap material with excitonic effects appearing as a shift in the spectral weight towards lower energies. For LiF, we can see that AGGA shifts the peak energies for $\mathbf{q} = 0.24\mathbf{\Gamma X}, 0.48\mathbf{\Gamma X}$ towards lower energies. But there are very little differences w.r.t. the ALDA results. Both ALDA and AGGA fail to capture the excitonic peak at 13 eV as neither has the correct $1/\mathbf{q}^2$ behavior in the long-wavelength limit. Outside the first BZ ($\mathbf{q} = 1.52\mathbf{\Gamma X}$), ALDA and AGGA exhibit similar behavior. For diamond, neither AGGA nor ALDA captures the shift in spectral weight as can be seen in Fig. 2(b). In fact there is little difference between the results obtained using the two approximations. To conclude

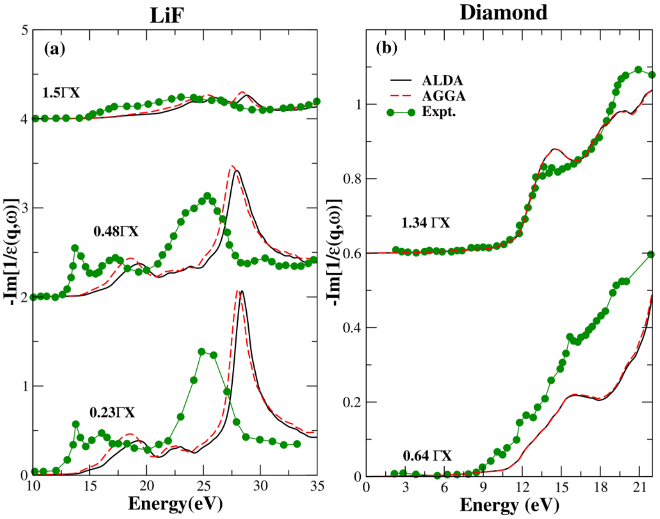

FIG. 2. Electron energy loss spectra given by imaginary part of the inverse dielectric tensor for different experimental values of **q** (indicated in the figure) as a function of photon energy for (a) LiF and (b) diamond, using the AGGA kernel (red dashed), the ALDA kernel (black line), and the experimental data [53] (green dots). Constrained by the k-point grid, the calculations are at **q** values as 0.24ΓX, 0.48ΓX, and 1.52ΓX for LiF and 0.64ΓX and 1.36ΓX for diamond.

TABLE I. Equilibrium lattice parameter a_0 (in Å) is calculated using the energy-volume curve fitted to the third order Birch-Murnaghan equation of state. The magnetic moments (in μ_B) calculated at these a_0 are given in columns 5 and 6. The experimental magnetic moments, $m_{\text{exp.}}$ and lattice parameters, a_0 (exp.), are also listed.

	a_0 (exp.)	a_0 (LDA)	a_0 (GGA)	$m_{\text{exp.}}$	m_{LDA}	m_{GGA}
Ni(fcc)	3.524[a]	3.436	3.527	0.60[b]	0.591	0.636
Co(fcc)	3.539[c]	3.429	3.525	1.52[d]	1.525	1.641
Fe(bcc)	2.8665[e]	2.743	2.836	2.08[f]	1.996	2.174

[a] Reference [62].
[b] Reference [63].
[c] Reference [64].
[d] Reference [65].
[e] Reference [66].
[f] Reference [67].

this section, for EELS, the additional **q** dependence of the AGGA kernel does not lead to any significant improvement over the ALDA kernel.

B. Spin excitation spectra

An *ab initio* computational method, given the atomic composition, should be able to predict the equilibrium geometry. Having found the minimum energy crystal structure from ground-state calculations, we can then calculate the excited state properties, all without reference to experimental data. Only those methods which follow this prescription can be considered fully predictive. However, as we wish to disentangle the effect of the kernel on the spin excitation spectra from that of the lattice spacing, we will first use experimental lattice spacings before exploring the dependence on equilibrium lattice constant.

The ground-state DFT calculations with experimental and optimized lattice parameters are summarized in Table I. From this we conclude that (i) GGA is very good in reproducing the structures of materials whereas (ii) LDA is better in predicting the magnetic moments.

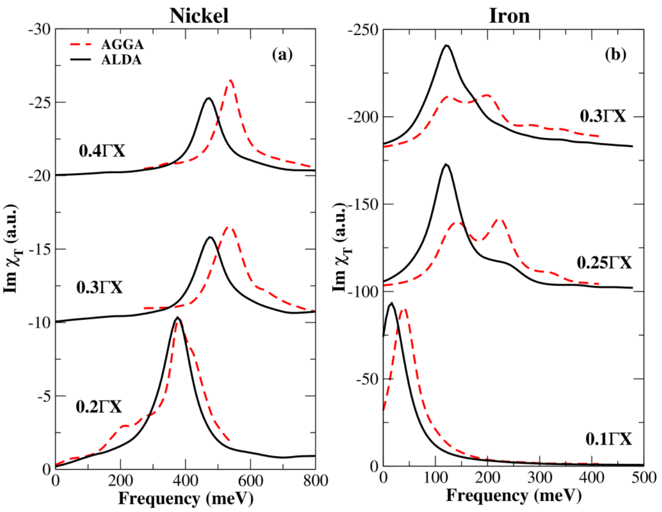

FIG. 4. The transverse response at certain **q** values for (a) nickel and (b) iron using ALDA (black lines) and AGGA (red dashed) kernels.

Within TDDFT the magnon spectra of a system can be calculated from the transverse response function $\chi^{-+}(\mathbf{q},\omega)$, which is found using the Dyson-like equation, Eq. (3). The excitations in $\chi^{-+}(\mathbf{q},\omega)$ originate from two sources: (1) renormalized poles of the KS response χ_0 corresponding to the Stoner continuum of single-particle spin-flips and (2) additional peaks created by the XC kernel corresponding to spin-wave excitations.

To find the magnon dispersion, we calculate $\text{Im}\{\chi^{-+}(\mathbf{q},\omega)\}$ for each **q** value, extract the magnon peak position, and then plot these as a function of **q**. This is shown in Fig. 3 for nickel, cobalt, and iron [at a_0(exp.) from Table I]. Experimental data and past ALDA results obtained

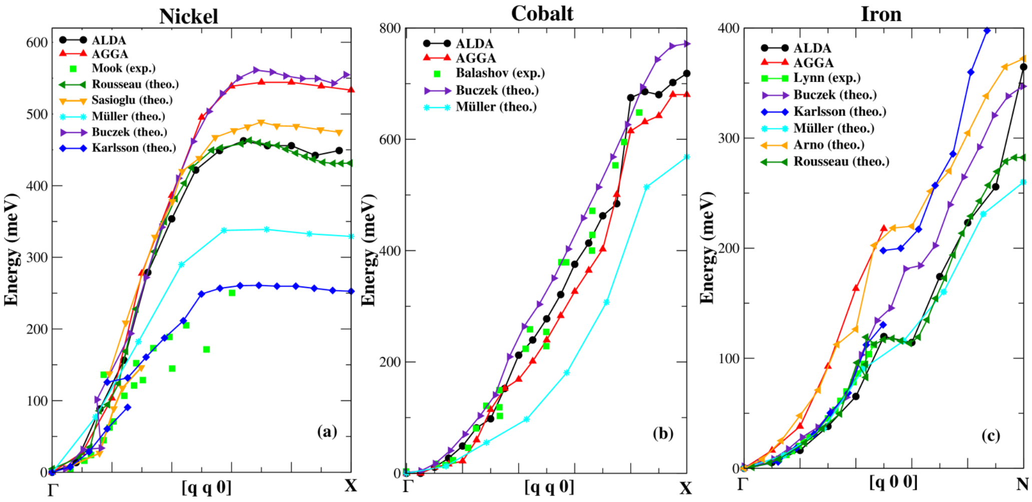

FIG. 3. Magnon dispersion spectrum for (a) fcc nickel, (b) fcc cobalt along the ΓX direction, and (c) bcc iron along the ΓN direction calculated using the ALDA kernel (black dots) and AGGA kernel (red triangles). A comparison is made with reported theoretical work [34,35,37,54,55] and also the experimental result (green squares) taken from Mook *et al.* [44,56] for nickel, Balashov *et al.* [57] for cobalt, and Lynn [58] for iron.

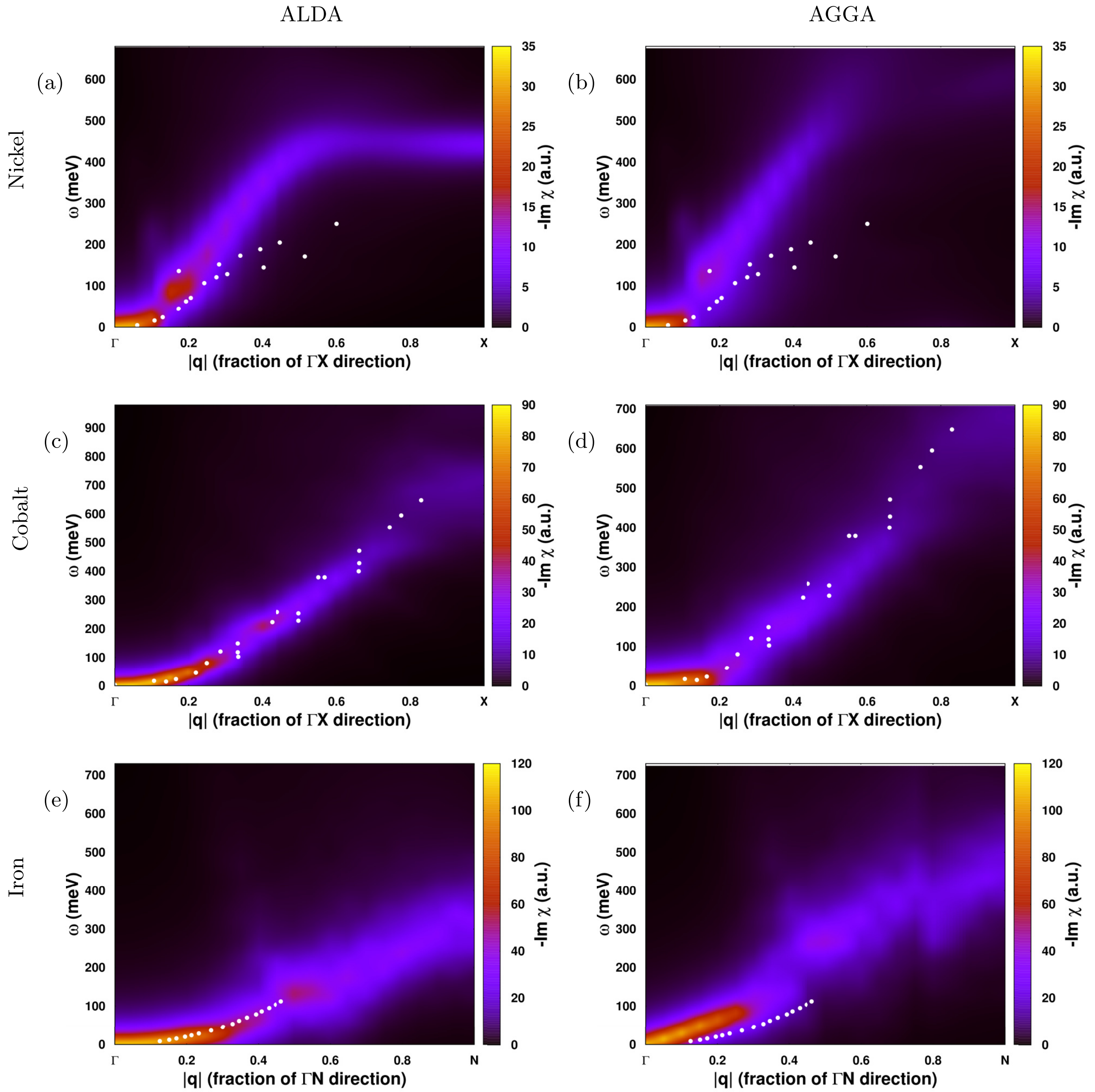

FIG. 5. The imaginary part of the interacting response of nickel, cobalt, and iron at the experimental lattice constants using the ALDA kernel [(a),(c),(e)] and the AGGA kernel [(b),(d),(f)] and the experimental results [56–58] (white dots).

within TDDFT or MBPT approach [34,37–40,54] are also presented. For Ref. [38], the LSDA corrected values have been taken. Our ALDA results are consistent with previously reported data. Most importantly we note that the AGGA kernel does not offer any improvement over ALDA spin excitation spectra. In the following, we will discuss each material individually before commenting on the general behavior of the AGGA XC kernel.

For Ni, Fig. 3(a), both the ALDA and the AGGA show quantitatively the same behavior from the BZ center to $|\mathbf{q}| = 0.4$. As we move further away from the zone center, the AGGA kernel tends to deviate from ALDA until it becomes ≈80 meV higher in energy at the zone boundary. For Co, Fig. 3(b), the experimental results are well captured by both ALDA and AGGA calculations. For Fe, Fig. 3(c), in contrast to ALDA which reproduces the experimental values, the AGGA dispersion overestimates the magnon energies. Beyond half ΓN, the transverse response function obtained using AGGA becomes too broad to assign a single energy to the excitation peaks although some features are still present, as can be seen in Fig. 4.

The strength and width of the peak in $\mathrm{Im}\{\chi^{-+}(\mathbf{q},\omega)\}$ is related to the scattering amplitude and lifetime of the magnon, respectively. To visualize how these properties

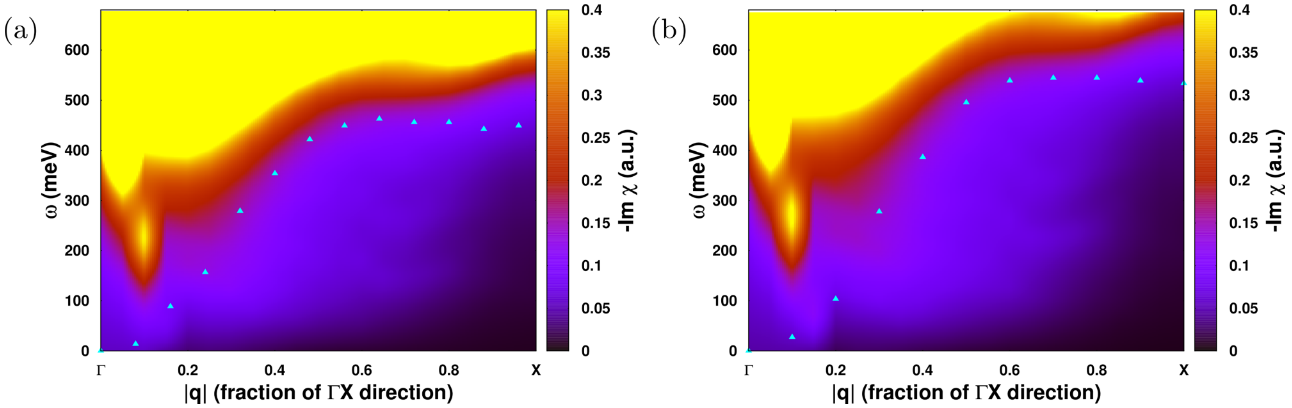

FIG. 6. Imaginary part of the noninteracting response function for nickel using (a) LDA and (b) GGA and also the corresponding ALDA and AGGA theoretical magnon spectra for comparison (cyan triangles).

change throughout the BZ, we can make a 2D contour plot of $\mathrm{Im}\{\chi^{-+}(\mathbf{q},\omega)\}$. These are shown for both ALDA and AGGA in Fig. 5 for Ni, Co, and Fe. Beginning again with Ni, we see that the peaks in $\mathrm{Im}\{\chi^{-+}(\mathbf{q},\omega)\}$ obtained by using ALDA [Fig. 5(a)] are stronger in intensity and better resolved than AGGA [Fig. 5(b)]. There exists a high probability of observing a magnon at the BZ boundary with ALDA whereas it is suppressed significantly beyond $\mathbf{q} = 0.5\mathbf{\Gamma X}$ with AGGA. We also observe a strong suppression in the magnon intensity between $|\mathbf{q}| = 0.1$ and 0.2 for both AGGA and ALDA [see Figs. 5(a) and 5(b)]. Experimentally, Paul *et al.* [56] measured a disruption to the magnon dispersion at $|\mathbf{q}| = 0.2$, where they observed a split into optical and acoustic branches. While neither ALDA nor AGGA shows two branches, both correctly predict an abrupt change in the magnon dispersion around this value of $\mathbf{q}$. This is due to the Stoner spin-flip transitions [Eq. (2)] having energy comparable to the magnon energy causing strong interference and intensity suppression [70] at these values of $\mathbf{q}$ (see Fig. 6).

In contrast to Ni, the experimental dispersion for fcc Co, obtained by Balashov *et al.* [57], along [100] does not show any optical branches. Both ALDA and AGGA behave the same and show good agreement with experiment, with AGGA being slightly lower in energy. Observing the full transverse response function over the whole BZ [Figs. 5(c) and 5(d)] we again see a reduction in the peak strength and suppression of the magnons by AGGA as compared to ALDA. Qualitatively, AGGA also reproduces the jump in magnon energy witnessed in experiments around $|\mathbf{q}| = 0.6$, although at a higher $|\mathbf{q}|$ value of 0.8.

For Fe, we see significant broadening in the AGGA transverse response for $|\mathbf{q}| > 0.5$ [Figs. 5(f) and 6(b)] to such an extent that it becomes impossible to assign a single peak position. We note that in Ref. [37] a jump to a higher branch occurs in this region. Experimental data reported in Ref. [71] do see magnon excitations in this region, although with a large full width at half maximum indicating strong suppression. This suppression can also be seen in our results due to interaction with the Stoner continuum.

We now test the predictive power of LDA and GGA by comparing their behavior for Ni, Co, and Fe at the experimental and optimized lattice parameters (see Fig. 7). We

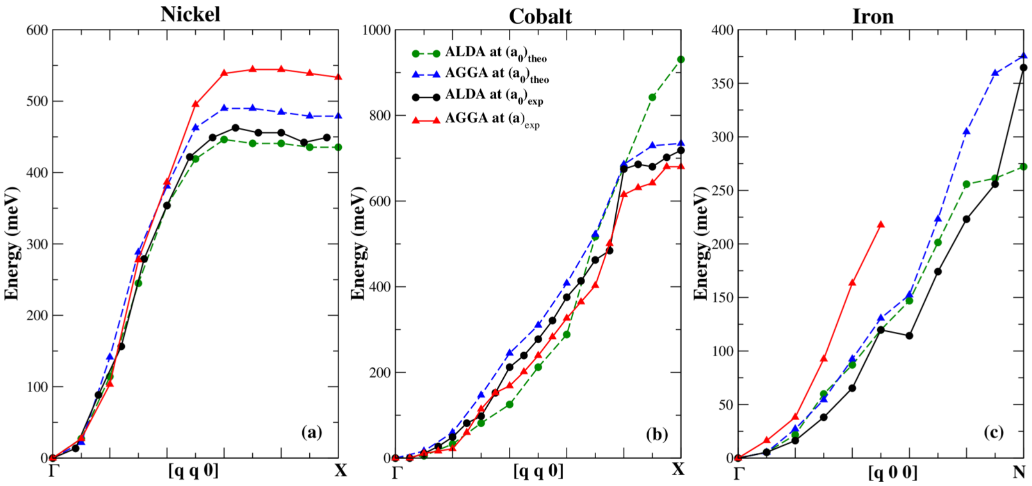

FIG. 7. The magnon spectrum with the theoretical and experimental lattice parameters for (a) fcc nickel, (b) fcc cobalt along the ΓX direction, and (c) bcc iron along the ΓN direction calculated using the ALDA kernel (dots) and AGGA kernel (triangles). The lattice parameters are given in Table I.

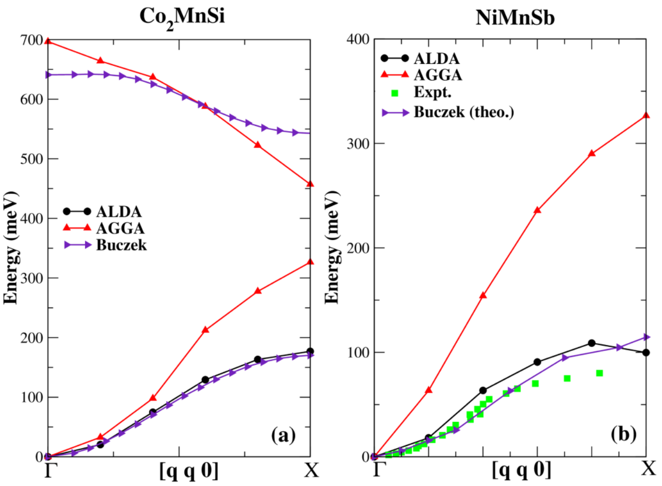

FIG. 8. (a) The magnon spectra of Co_2MnSi using the ALDA (black dots) and AGGA (red triangles) kernels and compared with Buczek calculations [68] with the ALDA kernel (violet triangle left). (b) The magnon spectra of NiMnSb using ALDA and AGGA kernel and the experimental results [69] (green squares).

find that the AGGA magnon spectra are more sensitive to the lattice parameters than the ALDA. In most cases, the AGGA results at the corresponding GGA parameter $(a_0)_{theo}$ are lower in energy than at $(a_0)_{exp}$, although still overestimated w.r.t. experiment.

Next we investigate Heusler and half-Heusler materials Co_2MnSi and NiMnSb which, due to their geometry of interlocking magnetic fcc lattices, can (in principle) have multiple magnon branches [68,72]. In Fig. 8, the AGGA magnon spectra of Co_2MnSi and NiMnSb are plotted along with the experimental and ALDA calculations. For Co_2MnSi [see Fig. 8(a)] both, an acoustic branch and an optical branch are observed. An increase in the energies of the acoustic branch is noted when compared with earlier ALDA results [68], based on loss function. However, energies of the optical branch with AGGA are within the same range as reported by Buczek [68] using ALDA. For NiMnSb [Fig. 8(b)], both ALDA and AGGA predict only an acoustic branch, as is also the case experimentally. This is likely due to Ni not possessing a strong local moment as most of the total moment is localized on the Mn atoms. In this case AGGA severely overestimates the magnon energies.

Finally, we offer the underlying explanation as to why AGGA tends to overestimate the magnon energies. The role of the XC kernel is to transform the excitation structure of $\mathrm{Im}\{\chi_0^{-+}\}$ into the true response. From the Stoner single-particle excitations, contained in $\mathrm{Im}\{\chi_0^{-+}\}$, it must create the magnon peak. At $\mathbf{q} = 0$, the gap in $\mathrm{Im}\{\chi_0^{-+}\}$ is related to the exchange splitting between spin-up and spin-down states. This splitting dictates the position of the Stoner continuum across the BZ. In Figs. 6(a) and 6(b), we plot $\mathrm{Im}\{\chi_0^{-+}\}$ for LDA and GGA, where we observe that the Stoner gap has increased by approximately 60 meV for nickel. This increment stems from the fact that GGA increases the exchange splitting in Ni by 59.9 meV compared to LDA, leading to the shift in Stoner continuum towards higher energies. At $\mathbf{q} = 0$, the symmetries of the response equation will enforce Goldstone's theorem, however the increase in the exchange splitting will cause the magnon energies also to increase as we move across the zone. This can be seen in Fig. 6 where both ALDA and AGGA have a similar behavior relative to the background Stoner excitations. Similar behavior was also observed for other materials, e.g., for Fe there is ≈150 meV increase and even a 50% increase of the LDA Stoner gap in χ_0^{-+} for the half-metal NiMnSb. The connection between the exchange splitting and the magnon energies was previously reported in Ref. [37] where the LDA value was artificially reduced leading to lower magnon energies. Given that LDA is well known to overestimate the exchange splitting, a further enhancement on going from LDA to GGA leads to large overestimation of the magnon energies.

V. CONCLUDING REMARKS

We have studied the charge and spin excitation spectra using the gradient dependent AGGA XC kernel within the linear response regime of TDDFT. The calculated EELS for LiF and diamond show that the AGGA kernel performs slightly better than the ALDA kernel, although, as would be expected, neither captures excitonic effects. For magnon dispersions, we found that AGGA, in general, does not systematically improve upon ALDA. This is due to the fact that the GGA XC functional overestimates the exchange splitting which in turn leads to higher magnon energies. Furthermore, the intensity of the peaks is greatly suppressed in the spectra obtained by the AGGA XC kernel due to interaction of spin waves with the Stoner continuum. This suppression is also observed in experiments, suggesting AGGA might provide better qualitative understanding than ALDA. Heusler materials consisting of multiple magnetic sublattices were also studied where it was found that AGGA is better at resolving higher-energy optical magnon branches.

In this work, we principally investigated the spin-spin response of collinear ferromagnetic systems, which greatly simplified the XC kernel. However, the AGGA XC kernel derived here is valid for all systems, and, in particular, has interesting terms for the spin-charge response and for noncollinear systems. This will be explored in future work.

It is important to test the performance of adiabatic functionals in TDDFT as their behavior can be quite different from the ground-state case. Only by implementing, assessing, and understanding this behavior can we gain insight into the relevant features necessary for accurate XC kernels, which can guide us towards improvement or in developing new approximations in TDDFT.

APPENDIX

For the spin polarized case, the exchange-correlation (XC) energy functional, $E_{\rm xc}$, depends on spin-up, $\rho_\alpha(\mathbf{r})$, spin-down, $\rho_\beta(\mathbf{r})$, densities and their gradients, $\nabla\rho_\alpha(\mathbf{r})$, $\nabla\rho_\beta(\mathbf{r})$. The XC potential, $v_{\rm xc}$, and the kernel, $f_{\rm xc}$, can be obtained by the first and second order functional derivative of $E_{\rm xc}$ with respect to the densities. Now adding variation in the two densities and their gradients and Taylor expanding one gets the XC energy density, e_{xc}, (up to first order only).

$$\begin{aligned}
&e_{\text{xc}}(\rho_\alpha(\mathbf{r})+\delta\rho_\alpha(\mathbf{r}),\,\rho_\beta(\mathbf{r})+\delta\rho_\beta(\mathbf{r}),\,\nabla\rho_\alpha(\mathbf{r})+\nabla\delta\rho_\alpha(\mathbf{r}),\,\nabla\rho_\beta(\mathbf{r})+\nabla\delta\rho_\beta(\mathbf{r}))\\
&\quad= e_{\text{xc}}(\rho_\alpha(\mathbf{r}),\,\rho_\beta(\mathbf{r}),\,\nabla\rho_\alpha(\mathbf{r}),\,\nabla\rho_\beta(\mathbf{r}))+\frac{\partial e_{\text{xc}}}{\partial\rho_\alpha}(\mathbf{r})\delta\rho_\alpha(\mathbf{r})+\frac{\partial e_{\text{xc}}}{\partial\rho_\beta}(\mathbf{r})\delta\rho_\beta(\mathbf{r})+\frac{\partial e_{\text{xc}}}{\partial\nabla\rho_\alpha}(\mathbf{r})\nabla\delta\rho_\alpha(\mathbf{r})+\frac{\partial e_{\text{xc}}}{\partial\nabla\rho_\beta}(\mathbf{r})\nabla\delta\rho_\beta(\mathbf{r})
\end{aligned}\tag{A1}$$

and

$$\begin{aligned}
&E_{\text{xc}}[\rho_\alpha(\mathbf{r})+\delta\rho_\alpha(\mathbf{r}),\,\rho_\beta(\mathbf{r})+\delta\rho_\beta(\mathbf{r}),\,\nabla\rho_\alpha(\mathbf{r})+\nabla\delta\rho_\alpha(\mathbf{r}),\,\nabla\rho_\beta(\mathbf{r})+\nabla\delta\rho_\beta(\mathbf{r})]\\
&\quad= E_{\text{xc}}[\rho_\alpha(\mathbf{r}),\,\rho_\beta(\mathbf{r}),\,\nabla\rho_\alpha(\mathbf{r}),\,\nabla\rho_\beta(\mathbf{r})]+\int d^3r\left[\frac{\partial e_{\text{xc}}}{\partial\rho_\alpha}(\mathbf{r})\delta\rho_\alpha(\mathbf{r})+\frac{\partial e_{\text{xc}}}{\partial\rho_\beta}(\mathbf{r})\delta\rho_\beta(\mathbf{r})+\frac{\partial e_{\text{xc}}}{\partial\nabla\rho_\alpha}(\mathbf{r})\nabla\delta\rho_\alpha(\mathbf{r})+\frac{\partial e_{\text{xc}}}{\partial\nabla\rho_\beta}(\mathbf{r})\nabla\delta\rho_\beta(\mathbf{r})\right]\\
&\delta E_{\text{xc}}=\int d^3r\left[\frac{\partial e_{\text{xc}}}{\partial\rho_\alpha}(\mathbf{r})\delta\rho_\alpha(\mathbf{r})+\frac{\partial e_{\text{xc}}}{\partial\rho_\beta}(\mathbf{r})\delta\rho_\beta(\mathbf{r})+\frac{\partial e_{\text{xc}}}{\partial\nabla\rho_\alpha}(\mathbf{r})\nabla\delta\rho_\alpha(\mathbf{r})+\frac{\partial e_{\text{xc}}}{\partial\nabla\rho_\beta}(\mathbf{r})\nabla\delta\rho_\beta(\mathbf{r})\right]
\end{aligned}\tag{A2}$$

As we know

$$\begin{aligned}
\delta E_{\text{xc}}=&\int d^3r\,v_{\text{xc}}^{\alpha}(\mathbf{r})\delta\rho_\alpha(\mathbf{r})+\int d^3r\,v_{\text{xc}}^{\beta}(\mathbf{r})\delta\rho_\beta(\mathbf{r})+\frac{1}{2}\int\int d^3r\,d^3r'\,f_{\text{xc}}^{\alpha\alpha}(\mathbf{r},\mathbf{r}')\delta\rho_\alpha(\mathbf{r})\delta\rho_\alpha(\mathbf{r}')\\
&+\frac{1}{2}\int\int d^3r\,d^3r'\,f_{\text{xc}}^{\alpha\beta}(\mathbf{r},\mathbf{r}')\delta\rho_\beta(\mathbf{r})\delta\rho_\alpha(\mathbf{r}')+\frac{1}{2}\int\int d^3r\,d^3r'\,f_{\text{xc}}^{\beta\alpha}(\mathbf{r},\mathbf{r}')\delta\rho_\alpha(\mathbf{r})\delta\rho_\beta(\mathbf{r}')\\
&+\frac{1}{2}\int\int d^3r\,d^3r'\,f_{\text{xc}}^{\beta\beta}(\mathbf{r},\mathbf{r}')\delta\rho_\beta(\mathbf{r})\delta\rho_\beta(\mathbf{r}'),
\end{aligned}\tag{A3}$$

so we could either expand Eq. (A1) to second order or use $v_{\text{xc}}^{\alpha,\beta}$, where $f_{\text{xc}}^{\alpha\alpha}$ is the change in v_{xc}^{α} when ρ_α changes and $f_{\text{xc}}^{\alpha\beta}$ is the change in v_{xc}^{α} when ρ_β changes, and similarly for the other spin channel. Using integration by parts in Eq. (A2), we obtain the XC potential for the two spin densities as:

$$v_{\text{xc}}^{\alpha}[\rho_\alpha,\rho_\beta,\nabla\rho_\alpha,\nabla\rho_\beta](\mathbf{r})=\frac{\partial e_{\text{xc}}}{\partial\rho_\alpha}(\mathbf{r})-\nabla_j\left[\frac{\partial e_{\text{xc}}}{\partial\nabla_j\rho_\alpha}(\mathbf{r})\right]\tag{A4}$$

and

$$v_{\text{xc}}^{\beta}[\rho_\alpha,\rho_\beta,\nabla\rho_\alpha,\nabla\rho_\beta](\mathbf{r})=\frac{\partial e_{\text{xc}}}{\partial\rho_\beta}(\mathbf{r})-\nabla_j\left[\frac{\partial e_{\text{xc}}}{\partial\nabla_j\rho_\beta}(\mathbf{r})\right].\tag{A5}$$

Now variation of v_{xc}^{α} w.r.t. ρ gives the kernels $f_{\text{xc}}^{\alpha\alpha}(\mathbf{r},\mathbf{r}')$ and $f_{\text{xc}}^{\alpha\beta}(\mathbf{r},\mathbf{r}')$ as

$$\begin{aligned}
\delta v_{\text{xc}}^{\alpha}(\mathbf{r})&=v_{\text{xc}}^{\alpha}[\rho_\alpha(\mathbf{r})+\delta\rho_\alpha(\mathbf{r}),\,\rho_\beta(\mathbf{r})+\delta\rho_\beta(\mathbf{r}),\,\nabla\rho_\alpha(\mathbf{r})+\nabla\delta\rho_\alpha(\mathbf{r}),\,\nabla\rho_\beta(\mathbf{r})+\nabla\delta\rho_\beta(\mathbf{r})]-v_{\text{xc}}^{\alpha}[\rho_\alpha,\rho_\beta,\nabla\rho_\alpha,\nabla\rho_\beta]\\
&=\left\{\frac{\partial^2 e_{\text{xc}}}{\partial\rho_\alpha^2}(\mathbf{r})\delta\rho_\alpha(\mathbf{r})+\left(\frac{\partial^2 e_{\text{xc}}}{\partial\nabla_k\rho_\alpha\partial\rho_\alpha}(\mathbf{r})\right)\nabla_k^r\delta\rho_\alpha(\mathbf{r})-\nabla_j\left[\left(\frac{\partial^2 e_{\text{xc}}}{\partial\rho_\alpha\partial\nabla_j\rho_\alpha}(\mathbf{r})\right)\delta\rho_\alpha(\mathbf{r})\right]\right.\\
&\quad\left.-\nabla_j\left[\left(\frac{\partial^2 e_{\text{xc}}}{\partial\nabla_k\rho_\alpha\partial\nabla_j\rho_\alpha}(\mathbf{r})\right)\nabla_k\delta\rho_\alpha(\mathbf{r})\right]\right\}+\left\{\frac{\partial^2 e_{\text{xc}}}{\partial\rho_\beta\partial\rho_\alpha}(\mathbf{r})\delta\rho_\beta(\mathbf{r})+\left(\frac{\partial^2 e_{\text{xc}}}{\partial\nabla_k\rho_\beta\partial\rho_\alpha}(\mathbf{r})\right)\nabla_k\delta\rho_\beta(\mathbf{r})\right.\\
&\quad\left.-\nabla_j\left[\left(\frac{\partial^2 e_{\text{xc}}}{\partial\rho_\beta\partial\nabla_j\rho_\alpha}(\mathbf{r})\right)\delta\rho_\beta(\mathbf{r})\right]-\nabla_j\left[\left(\frac{\partial^2 e_{\text{xc}}}{\partial\nabla_k\rho_\beta\partial\nabla_j\rho_\alpha}(\mathbf{r})\right)\nabla_k\delta\rho_\beta(\mathbf{r})\right]\right\}\\
&=\int f_{\text{xc}}^{\alpha\alpha}(\mathbf{r},\mathbf{r}')\delta\rho_\alpha(\mathbf{r}')d^3r'+\int f_{\text{xc}}^{\alpha\beta}(\mathbf{r},\mathbf{r}')\delta\rho_\alpha(\mathbf{r}')d^3r'.
\end{aligned}\tag{A6}$$

Solving each term separately by introducing an integration with a delta function, we obtain the kernels $f_{\text{xc}}^{\alpha\alpha}(\mathbf{r},\mathbf{r}')$ and $f_{\text{xc}}^{\alpha\beta}(\mathbf{r},\mathbf{r}')$

$$f_{\text{xc}}^{\alpha\alpha}(\mathbf{r},\mathbf{r}')=\delta(\mathbf{r}-\mathbf{r}')\left[\frac{\partial^2 e_{xc}}{\partial\rho_\alpha\partial\rho_\alpha}(\mathbf{r})-\left(\nabla_k\frac{\partial^2 e_{xc}}{\partial\nabla_k\rho_\alpha\partial\rho_\alpha}(\mathbf{r})\right)\right]-\nabla_k'\left[[\nabla_j'\delta(\mathbf{r}-\mathbf{r}')]\left(\frac{\partial^2 e_{xc}}{\partial\nabla_k\rho_\alpha\partial\nabla_j\rho_\alpha}(\mathbf{r}')\right)\right]\tag{A7}$$

$$\begin{aligned}
f_{\text{xc}}^{\alpha\beta}(\mathbf{r},\mathbf{r}')=&\,\delta(\mathbf{r}-\mathbf{r}')\left\{\frac{\partial^2 e_{\text{xc}}}{\partial\rho_\beta\partial\rho_\alpha}(\mathbf{r}')\right\}-\left\{[\nabla_j'\delta(\mathbf{r}-\mathbf{r}')]\left(\frac{\partial^2 e_{\text{xc}}}{\partial\rho_\alpha\partial\nabla_j\rho_\beta}(\mathbf{r})\right)\right\}\\
&+\left\{[\nabla_j'\delta(\mathbf{r}-\mathbf{r}')]\left(\frac{\partial^2 e_{\text{xc}}}{\partial\rho_\beta\partial\nabla_j\rho_\alpha}(\mathbf{r}')\right)\right\}-\nabla_k'\left\{[\nabla_j'\delta(\mathbf{r}-\mathbf{r}')]\left(\frac{\partial^2 e_{\text{xc}}}{\partial\nabla_k\rho_\beta\partial\nabla_j\rho_\alpha}(\mathbf{r}')\right)\right\}.
\end{aligned}\tag{A8}$$

For noncollinear systems, the kernel comprises charge-charge $f_{\rm xc}^{00}$, charge-spin $f_{\rm xc}^{0i}$, and spin-spin $f_{\rm xc}^{ij}$ terms which consist of the above $f_{\rm xc}^{\alpha\alpha}$ and $f_{\rm xc}^{\alpha\beta}$ terms:

$$f_{\rm xc}^{00} = \frac{1}{4}\left[f_{\rm xc}^{\uparrow\uparrow}(\mathbf{r},\mathbf{r}') + f_{\rm xc}^{\uparrow\downarrow}(\mathbf{r},\mathbf{r}') + f_{\rm xc}^{\downarrow\uparrow}(\mathbf{r},\mathbf{r}') + f_{\rm xc}^{\downarrow\downarrow}(\mathbf{r},\mathbf{r}')\right] \tag{A9}$$

$$f_{\rm xc}^{0i}(\mathbf{r},\mathbf{r}') = \frac{1}{4}\left[f_{\rm xc}^{\uparrow\uparrow}(\mathbf{r},\mathbf{r}') - f_{\rm xc}^{\uparrow\downarrow}(\mathbf{r},\mathbf{r}') + f_{\rm xc}^{\downarrow\uparrow}(\mathbf{r},\mathbf{r}') - f_{\rm xc}^{\downarrow\downarrow}(\mathbf{r},\mathbf{r}')\right]\hat{m}_i(\mathbf{r}') \tag{A10}$$

$$f_{\rm xc}^{i0}(\mathbf{r},\mathbf{r}') = f_{\rm xc}^{0i}(\mathbf{r}',\mathbf{r}) \tag{A11}$$

$$f_{\rm xc}^{ij}(\mathbf{r},\mathbf{r}') = \frac{1}{4}\left[f_{\rm xc}^{\uparrow\uparrow}(\mathbf{r},\mathbf{r}') - f_{\rm xc}^{\uparrow\downarrow}(\mathbf{r},\mathbf{r}') - f_{\rm xc}^{\downarrow\uparrow}(\mathbf{r},\mathbf{r}') + f_{\rm xc}^{\downarrow\downarrow}(\mathbf{r},\mathbf{r}') - \frac{|\mathbf{B}_{\rm xc}|}{|\mathbf{m}|}\right]\hat{m}_i(\mathbf{r})\hat{m}_j(\mathbf{r}') + \frac{|\mathbf{B}_{\rm xc}|}{|\mathbf{m}|}I_3, \tag{A12}$$

where I_3 is the 3×3 identity matrix, $\hat{m}$ is the unit magnetization vector, $|\mathbf{B}_{\rm xc}|$ is the magnitude of magnetic field, and $|\mathbf{m}|$ is the magnitude of the magnetization.

[1] U. Bovensiepan, Nat. Phys. **5**, 461 (2009), and references therein.

[2] E. Beaurepaire, J.-C. Merle, A. Daunois, and J.-Y. Bigot, Phys. Rev. Lett. **76**, 4250 (1996).

[3] S. Sharma, L. Nordström, and B. Johansson, Phys. Rev. B **66**, 195101 (2002).

[4] C. Kittel, *Introduction to Solid State Physics*, 6th ed. (John Wiley & Sons, Inc., New York, 1986).

[5] R. Mondal, M. Berritta, and P. M. Oppeneer, Phys. Rev. B **94**, 144419 (2016).

[6] W. Heisenberg, Z. Phys. **49**, 619 (1928).

[7] E. Runge and E. K. U. Gross, Phys. Rev. Lett. **52**, 997 (1984).

[8] S. Sharma, J. K. Dewhurst, and E. K. U. Gross, *First Principles Approaches to Spectroscopic Properties of Complex Materials*, edited by C. Di Valentin, S. Botti, and M. Cococcioni, Topics in Current Chemistry **347**, 235 (2014).

[9] P. Elliott, F. Furche, and K. Burke, in *Excited States from Time-Dependent Density Functional Theory*, edited by K. B. Lipkowitz, and T. R. Cundari, Reviews in Computational Chemistry, Vol. 26 (Wiley, Hoboken, NJ, 2009), Chap. 3, pp. 91–165.

[10] C. A. Ullrich, *Time-Dependent Density-Functional Theory* (Oxford University Press, New York, 2014).

[11] S. Sharma, J. K. Dewhurst, A. Sanna, and E. K. U. Gross, Phys. Rev. Lett. **107**, 186401 (2011).

[12] P. Elliott, T. Müller, J. K. Dewhurst, S. Sharma, and E. K. U. Gross, Sci. Rep. **6**, 38911 (2016).

[13] P. Elliott, K. Krieger, J. K. Dewhurst, S. Sharma, and E. K. U. Gross, New J. Phys. **18**, 013014 (2016).

[14] C. Andrea Rozzi, S. Maria Falke, N. Spallanzani, A. Rubio, E. Molinari, D. Brida, M. Maiuri, G. Cerullo, H. Schramm, J. Christoffers, and C. Lienau, Nat. Commun. **4**, 1602 (2013).

[15] J. Simoni, M. Stamenova, and S. Sanvito, Phys. Rev. B **96**, 054411 (2017).

[16] K. Krieger, P. Elliott, T. Müller, N. Singh, J. K. Dewhurst, E. K. U. Gross, and S. Sharma, J. Phys.: Condens. Matter **29**, 224001 (2017).

[17] J. K. Dewhurst, P. Elliott, S. Shallcross, E. K. U. Gross, and S. Sharma, Nano Lett. **18**, 1842 (2018).

[18] V. Shokeen, M. Sanchez Piaia, J.-Y. Bigot, T. Müller, P. Elliott, J. K. Dewhurst, S. Sharma, and E. K. U. Gross, Phys. Rev. Lett. **119**, 107203 (2017).

[19] K. Krieger, J. K. Dewhurst, P. Elliott, S. Sharma, and E. K. U. Gross, J. Chem. Theory Comput. **11**, 4870 (2015).

[20] J. P. Perdew and K. Schmidt, in *Density Functional Theory and its Application to Materials*, edited by V. Van Doren, C. Van Alsenoy, and P. Geerlings, AIP Conf. Proc. No. 577 (AIP, New York, 2001), p. 1.

[21] M. Panholzer, M. Gatti, and L. Reining, Phys. Rev. Lett. **120**, 166402 (2018).

[22] A. V. Terentjev, L. A. Constantin, and J. M. Pitarke, Phys. Rev. B **98**, 085123 (2018).

[23] J. Paier, M. Marsman, and G. Kresse, Phys. Rev. B **78**, 121201 (2008).

[24] S. Refaely-Abramson, M. Jain, S. Sharifzadeh, J. B. Neaton, and L. Kronik, Phys. Rev. B **92**, 081204 (2015).

[25] C. A. Ullrich and Z. Yang, Top Curr. Chem. **368**, 185 (2016).

[26] S. Sharma, J. K. Dewhurst, A. Sanna, A. Rubio, and E. K. U. Gross, New J. Phys. **14**, 053052 (2012).

[27] A. Marini, R. Del Sole, and A. Rubio, Phys. Rev. Lett. **91**, 256402 (2003).

[28] M. Hellgren and U. von Barth, J. Chem. Phys. **131**, 044110 (2009).

[29] L. Reining, V. Olevano, A. Rubio, and G. Onida, Phys. Rev. Lett. **88**, 066404 (2002).

[30] S. Botti, F. Sottile, N. Vast, V. Olevano, L. Reining, H.-C. Weissker, A. Rubio, G. Onida, R. Del Sole, and R. W. Godby, Phys. Rev. B **69**, 155112 (2004).

[31] F. Sottile, K. Karlsson, L. Reining, and F. Aryasetiawan, Phys. Rev. B **68**, 205112 (2003).

[32] F. Sottile, V. Olevano, and L. Reining, Phys. Rev. Lett. **91**, 056402 (2003).

[33] V. U. Nazarov and G. Vignale, Phys. Rev. Lett. **107**, 216402 (2011).

[34] P. Buczek, A. Ernst, and L. M. Sandratskii, Phys. Rev. B **84**, 174418 (2011).

[35] B. Rousseau, A. Eiguren, and A. Bergara, Phys. Rev. B **85**, 054305 (2012).

[36] F. Essenberger, S. Sharma, J. K. Dewhurst, C. Bersier, F. Cricchio, L. Nordström, and E. K. U. Gross, Phys. Rev. B **84**, 174425 (2011).

[37] K. Karlsson and F. Aryasetiawan, J. Phys.: Condens. Matter **12**, 7617 (2000).

[38] M. C. T. D. Müller, C. Friedrich, and S. Blügel, Phys. Rev. B **94**, 064433 (2016).

[39] S. Y. Savrasov, Phys. Rev. Lett. **81**, 2570 (1998).

[40] S. V. Halilov, A. Y. Perlov, P. M. Oppeneer, and H. Eschrig, Europhys. Lett. **39**, 91 (1997).

[41] L. Stixrude, R. E. Cohen, and D. J. Singh, Phys. Rev. B **50**, 6442 (1994).

[42] S. Raghu, S. B. Chung, X.-L. Qi, and S.-C. Zhang, Phys. Rev. Lett. **104**, 116401 (2010).

[43] J. Lafuente-Bartolome, I. G. Gurtubay, and A. Eiguren, Phys. Rev. B **96**, 035416 (2017).

[44] J. W. Lynn and H. A. Mook, Phys. Rev. B **23**, 198 (1981).

[45] D. Egli and S. R. Billeter, Phys. Rev. B **69**, 115106 (2004).

[46] A. Dal Corso, S. Baroni, and R. Resta, Phys. Rev. B **49**, 5323 (1994).

[47] J. Kubler, K.-H. Hock, J. Sticht, and A. R. Williams, J. Phys. F **18**, 469 (1988).

[48] `elk.sourceforge.net`.

[49] J. P. Perdew and Y. Wang, Phys. Rev. B **45**, 13244 (1992).

[50] J. P. Perdew, K. Burke, and M. Ernzerhof, Phys. Rev. Lett. **77**, 3865 (1996).

[51] H. C. Kandpal, G. H. Fecher, C. Felser, and G. Schönhense, Phys. Rev. B **73**, 094422 (2006).

[52] R. Helmholdt, R. de Groot, F. Mueller, P. van Engen, and K. Buschow, J. Magn. Magn. Mater. **43**, 249 (1984).

[53] W. A. Caliebe, J. A. Soininen, E. L. Shirley, C.-C. Kao, and K. Hämäläinen, Phys. Rev. Lett. **84**, 3907 (2000).

[54] E. Şaşıoğlu, A. Schindlmayr, C. Friedrich, F. Freimuth, and S. Blügel, Phys. Rev. B **81**, 054434 (2010).

[55] A. Schindlmayr, C. Friedrich, E. Şaşıoğlu, and S. Blügel, Z. Phys. Chem. **224**, 357 (2010).

[56] H. A. Mook and D. M. Paul, Phys. Rev. Lett. **54**, 227 (1985).

[57] T. Balashov, STM and STS investigation of magnetic nanostructures, inelastic magnetic excitations, magneto-electric coupling, surface science., Ph.D. thesis, Physikalisches Institut, Universität Karlsruhe (TH), Karlsruhe, 2009.

[58] J. W. Lynn, Phys. Rev. B **11**, 2624 (1975).

[59] S. Sharma, J. K. Dewhurst, S. Shallcross, G. K. Madjarova, and E. K. U. Gross, J. Chem. Theory Comput. **11**, 1710 (2015).

[60] D. Azhikodan, T. Nautiyal, S. Shallcross, and S. Sharma, Sci. Rep. **6**, 37075 (2016).

[61] P. Ghosez, X. Gonze, and R. W. Godby, Phys. Rev. B **56**, 12811 (1997).

[62] A. Taylor, J. Inst. Met. **77**, 585 (1950).

[63] V. Iota, J.-H. P. Klepeis, C.-S. Yoo, J. Lang, D. Haskel, and G. Srajer, Appl. Phys. Lett. **90**, 042505 (2007).

[64] F. Vincent and M. Figlarz, Weekly Records of the Academy of science series C **264**, 1270 (1967).

[65] M. B. Stearns, in *Magnetic Properties in Metals*, New Series, edited by H. Wijn and Landolt-Börnstein (Springer, Berlin, 1986), Vol. 3.

[66] R. Kohlhaas, P. Dünner, and S.N, Z. Angew. Phys. **23**, 245 (1967).

[67] D. Bonnenberg, K. Hempel, H. Wijn, in *Magnetic Properties in Metals*, New Series, edited by H. Wijn and Landolt-Börnstein (Springer, Berlin, 1986), Vol. 3.

[68] P. Buczek, A. Ernst, P. Bruno, and L. M. Sandratskii, Phys. Rev. Lett. **102**, 247206 (2009).

[69] C. Hordequin, J. Pierre, and R. Currat, Physica B: Condensed Matter **234-236**, 605 (1997).

[70] H. Kronmüller and S. Parkin, *Handbook of Magnetism and Advanced Magnetic Materials* (Wiley, Chichester, England, 2007), Vol. 1.

[71] T. G. Perring, A. T. Boothroyd, D. M. Paul, A. D. Taylor, R. Osborn, R. J. Newport, J. A. Blackman, and H. A. Mook, J. Appl. Phys. **69**, 6219 (1991).

[72] E. Şaşıoğlu, L. M. Sandratskii, P. Bruno, and I. Galanakis, Phys. Rev. B **72**, 184415 (2005).